International Journal of Biological Macromolecules 191 (2021) 1137–1150

Contents lists available at ScienceDirect

International Journal of Biological Macromolecules

journal homepage: www.elsevier.com/locate/ijbiomac

Synthesis of gold and silver nanoparticles by use of arabinoglucan from *Lallemantia royleana*

Fozia Iram [a], Abida Yasmeen [a], Shazma Massey [b], Mohammad S. Iqbal [b,*], Sumreen Asim [c], Misbah Irshad [d], Hina Zahid [b], Athar Y. Khan [b], Syed G.T. Kazimi [e]

[a] Department of Chemistry, LCW University, Lahore 54600, Pakistan
[b] Department of Chemistry, Forman Christian College, Lahore 54600, Pakistan
[c] Department of Chemistry, Khawaja Fareed University of Engineering and Information Technology, Rahim Yar Khan 64200, Pakistan
[d] Department of Chemistry, Division of Science and Technology, University of Education, Lahore 54770, Pakistan
[e] Department of Chemistry, University of Sargodha, Sargodha, Pakistan

ARTICLE INFO

Keywords:
Lallemantia royleana
Hemicelluloses
Gold nanoparticles
Silver nanoparticles
Carbohydrate polymers

ABSTRACT

Highly stable gold and silver nanoparticles were synthesized by use of an arabinoglucan from *Lallemantia royleana* seeds without additional use of reducing or stabilizing agents. The mechanism involved the reduction potential of the hemicellulose as verified by cyclic voltammetry. The arabinoglucan used was substantially free from ferulic acid and phenolic content, suggesting the inherent reducing potential of arabinoglucan for gold and silver ions. The synthesized nanoparticles exhibited surface plasmon resonance maxima at 515 nm (gold) and 397 nm (silver) corresponding to sizes of 10 nm and 8 nm, respectively. The zeta potential values were −24.1 mV (gold) and −22.3 mV (silver). The silver nanoparticles showed potential for application in surface-enhanced Raman spectroscopy. Gold nanoparticles were found to be non-toxic, whereas silver nanoparticles exhibited dose-dependent biological activities and found to be cytotoxic against brine shrimps and HeLa cell lines and the tumours caused by *A. tumefaciens*.

1. Introduction

Nanoparticles (NPs) of gold and silver are of great interest for pharmaceutical and biomedical applications because of their resistance to oxidation and unique optical properties [1–5]. Generally synthesis of metal NPs involves the use of hazardous reducing agents such as hydrazine, sodium citrate and sodium borohydride [6–8]. Although, the excess amount is washed out but this process does not rule out the presence of residual amount of the toxic agents. For biomedical applications the particles need to be absolutely free from toxic materials. In order to ensure this the use of toxic reducing and capping agents in the synthesis of NPs must be eliminated. Therefore, nanochemists are in search of biocompatible and biodegradable materials for use as reducing and capping agents. Among several natural products, hemicelluloses have been reported to be suitable for such applications [9–12].

Hemicelluloses are major class of polysaccharides and second most abundant biomaterials in nature after cellulose. Glucans are hemicelluloses comprising of various combinations of glucose units with other monosaccharides, depending on source and extraction process used [13]. Most of the new work is focussing on use of natural renewable materials for synthesis of metal NPs because of their abundant availability and benign nature.

Generally glucans are composed of glucose monomers linked through β-(1–3) and β-(1–4) glycosidic bonds. The β-(1–3) linkages are separated by 2 or 3 β-(1–4) linkages in varying ratios [14–16]. Keeping in view the abundant availability (from renewable sources) and high biocompatibility of hemicelluloses, we have reported the use of arabonoxylans and glucoxylans from food materials for synthesis of gold or silver NPs [9,10,17]. In these and other studies it was postulated that hemicelluloses hydrolyse to some extent into monosaccharaides which in turn exist in cyclic and acyclic (aldehyde form) forms in equilibrium in aqueous medium, [11,18] where the aldehyde group becomes available for the reduction of metal ions.

Based on the promising results of our previous studies we now report

* Corresponding author.
E-mail addresses: fozia.iram@lcwu.edu.pk (F. Iram), abida.yasmeen@lcwu.edu.pk (A. Yasmeen), shazmaazeem@fccollege.edu.pk (S. Massey), saeediqbal@fccollege.edu.pk (M.S. Iqbal), sumreen.asim@kfueit.edu.pk (S. Asim), misbahirshad@ue.edu.pk (M. Irshad), atharkhan@fcollege.edu.pk (A.Y. Khan), gohar.taqi@uos.edu.pk (S.G.T. Kazimi).

https://doi.org/10.1016/j.ijbiomac.2021.09.096
Received 1 June 2021; Received in revised form 9 August 2021; Accepted 15 September 2021
Available online 24 September 2021
0141-8130/© 2021 Elsevier B.V. All rights reserved.

the use of arabinoglucan (Ara-Glc) from *Lallementia roylena* (*LR*) seeds for the synthesis of gold and silver NPs without any additional reducing and stabilizing agent. *LR* is a food material from renewable sources and abundantly available in most parts of the world. The monosaccharide composition of the hemicellulose isolated from seeds of *LR* is already reported [19] as: glucose (63.90), arabinose (16.39), rhamose (10.97), galactose (7.55) and xylose (1.19%). In order to practically verify the mechanism of reduction process, experiments were carried out to determine redox potentials of the (Ara-Glc) by cyclic voltammetry. The other focus of the study was to look at the use of Ara-Glc stabilized gold and silver NPs as probes for surface-enhanced Raman spectroscopy (SERS). The hypothesis of research was that hemicelluloses possess inherent reducing and stabilizing potential in synthesis of metal NPs.

2. Experimental

2.1. Materials

The materials used in this study were: $HAuCl_4{\cdot}3H_2O$, $AgNO_3$, NaOH, Na_2CO_3, HNO_3, HCl and Folin Reagent from E. Merck, Germany; carbon coated copper grids (AGS160) from Agar Scientific and dialysis Membrane-110, molecular weight cut off 12000–14000 Da, pore size: 2.4 nm from HiMedia laboratories India. Coomassie Brilliant Blue R-250, neutral red, glacial acetic acid, disodium hydrogen phosphate, dimethyl sulfoxide (DMSO), glycerol and sodium dodecyl sulfate (SDS) were of analytical grade from sigma Aldrich (USA); HeLa cells (ATCC: CCL 2) from Flow Labs (London, UK); fetal bovine serum (FBS), Dulbecco's Modified Eagle Medium (DMEM) and penicillin-streptomycin were from Gibco, USA. The neutral Ara-Glc from *LR* seeds (M_w 3.5 × 10^6; consisting of glucose 63.90, arabinose 16.39, rhamose 10.97, galactose 7.55, xylose 1.19; moisture 13.67 ± 1.7%) was a gift from Ms. Shumaila Rao [19]. All the chemicals were used without further purification. Nanopure® water was used throughout this work.

2.2. Determination of phenolic content

The Ara-Glc was analysed by Folin-Ciocalteu method [20] for any phenolic content. For this the Ara-Glc (30 mg) was dispersed in water; the mixture was filtered and final volume of the filtrate was made to 10 mL. To this 1.5 mL $NaCO_3$ solution (20% w/v) and 0.5 mL of Folin reagent were added. The solution was incubated for 1 h at 25 °C and absorbance was recorded at 650 nm using water as the blank. The calibration curve was constructed by using 0.1–20 mgL^{-1} solutions of phenol. The measurements were performed in triplicate.

2.3. Determination of redox potentials of the Ara-Glc by cyclic voltammetry

The redox potentials of the Ara-Glc under investigation were determined by cyclic voltammetry (CV). The measurements were performed by using a three-electrode cell on potentiostat (eDAQ, Australia). Glassy carbon (electrode area = 0.00785 cm^2), platinum wire and Ag/AgCl were used as the working (WE), counter (CE) and reference (RE) electrodes respectively. NaOH (0.1 M) was used as the electrolyte. The electrolyte solution was purged with argon for about 10 min to expel air out and maintain an inert atmosphere. The cyclic voltammograms were recorded at 20 mV s^{-1}.

2.4. Synthesis of NPs

Solutions of $HAuCl_4{\cdot}3H_2O$ (1.0 mM) and $AgNO_3$ (1.0 mM) were prepared, separately, in water and labelled as solution A. 0.2% w/v solution of the Ara-Glc was prepared in water and labelled as B. To the 20 mL solution, varying amounts (2–20 mL) of solution B were added under vigorous stirring at varying temperatures (25–80 °C) and pH (3.5–12). The pH values of the mixtures after addition of the metal salts were 3.2 ($HAuCl_4$) and 4.3 ($AgNO_3$), which were appropriately adjusted by use of NaOH (0.1 M) solution. The NaOH solution did not show any redox activity in a separate experiment. The total volume of the mixture was made upto 40 mL by additional amount of water. The amount of Ara-Glc, temperature and pH were optimized. A change in colour (yellow to purple/red in case of AuNPs; colourless to yellow-brown in case of AgNPs) was observed within 10–60 min depending upon the amount of the Ara-Glc, pH and temperature. The resultant NPs were purified from large aggregates, and unreacted suspension by vacuum filtration and dialyzed for 24 h to remove excessive $HAuCl_4{\cdot}3H_2O$ or $AgNO_3$.

2.5. Characterization of NPs

The NPs were characterized by surface plasmon resonance (SPR), pXRD, electron microscopy, dynamic light scattering (DLS), zeta potential measurements and Raman spectroscopy. The SPR spectra were recorded in the 300–800 nm range after four-time dilution of the suspensions of gold and silver NPs with water. The (Ara-Glc) solution without NPs was used as the reference. Size of AuNPs was calculated from SPR spectra by using Eq. (1) for particles in the range 35–100 nm and Eq. (2) for particles 5–30 nm [21].

$$d\ (nm) = \frac{ln\left(\frac{\lambda_{spr}-\lambda_0}{L_1}\right)}{L_2} \tag{1}$$

where, d = diameter of the AuNP, λ_{spr} = wavelength of maximum absorption of the sample $\lambda_0 = 512$, $L_1 = 6.53$ and $L_2 = 0.0216$.

$$d = \left(\frac{A_{spr}\left(5.89 \times 10^{-6}\right)}{C_{Au} exp\ (c_1)}\right)^{\frac{1}{C_2}} \tag{2}$$

where $C_1 = -4.70$, $C_2 = 0.314$, A_{abs} = absorbance at λ_{max}. The extinction coefficient (ε) of AuNPs was estimated from the table provided by Sigma Aldrich [22]. Whereas, size and extinction coefficients of AgNPs were determined by a reported method [23] from the SPR spectra. Stability of the synthesized particles was studied by recording SPR spectra at different intervals of time extending upto four years.

For pXRD analysis, the samples were prepared by centrifugation at 5000 rpm for 20 min, the pellet formed was dried in an oven at 50 °C to a constant weight. The pXRD spectra of dried samples were recorded on Bruker D8 Discover (Germany) diffractometer using with monochromatic Cu-Kα radiation (λ = 1.5406 Å) operating at 40 kV and 30 mA. The data were collected over 2θ scanning between 10° and 80°.

For electron microscopy the sample suspensions of the NPs were diluted ten times with water and centrifuged at 5000 rpm for 30 min. The pallet formed was re-dispersed in water under sonication and centrifuged again. This process was repeated three times. The pallet thus obtained was dispersed in water and a drop of the solution was placed on a carbon coated grid and dried for imaging. SEM images were obtained by Jeol 7000F SEM (Jeol, Japan) equipped with EDS facility for elemental analysis and TEM images were obtained by JEM-1200EX (Jeol, Japan) TEM at an accelerating voltage of 120 kV. For AFM imaging a drop of suspensions of the NPs diluted 1000 times with water was placed on a silicon wafer (approximately 20 mm × 20 mm) and dried at 35 °C for about 15 min. AFM images were recorded at 2.44 Hz scan rate by Nanoscope IIIa atomic force microscope (Digital Instruments, USA) in the contact mode using cantilevers with oxide-sharpened silicon nitride probes (NP-S1, Veeco, USA).

The hydrodynamic diameter of the particles was determined using 100 time dilutions of the suspensions of the NPs in a disposable cuvette, after equilibration for 2–3 min at 21 °C. Ten replicates of each sample were analysed by He-Ne laser high performance particle sizer (NanoZS90 HPPS 5001; Malvern, UK) and mean ± SD values were reported. Zeta potential was determined by use of folded capillary cells (DTS 1060) avoiding any air bubbles. The results were reported as mean

± SD of ten replicates.

The Raman spectra were recorded in the range 1800–200 cm^{-1} by placing a drop of NPs solution on a glass slide using confocal Raman microscope (Olympus, IX71, Horiba Jovin Yvon, USA) equipped with an argon-ion 8 mW laser (Coherent, Innova 70 C series) as excitation source at 532 nm.

2.6. Bioassays

2.6.1. Antibacterial assay

The synthesized NPs were tested for antimicrobial activity by well-diffusion method against Gram-negative strains (*E. coli*, *A. tumefaciens* and *P. aeruginosa*) and Gram-positive strains [24]. The pure bacterial cultures were sub-cultured on nutrient broth at 37 °C for 24 h. After incubation bacterial subcultures (100 μL each) were mixed with 50 mL sterilized molten nutrient agar at 50 °C, and transferred to petri plates. Once the medium solidified, wells of 8 mm in diameter were made with sterile borer and labelled. The AgNPs (10 and 30 nm: 180 μg mL^{-1}) and AuNPs (10 and 30 nm: 180 μg mL^{-1}) were loaded in separate wells. Roxithromycin (100 ppm, 10 μL) was used as a positive control (C-1), whereas water (C-2) and pure hemicellulose (C-3; 670 μg mL^{-1}) were negative controls. Aqueous $HAuCl_4{\cdot}3H_2O$ (1.0 mM) and $AgNO_3$ (1.0 mM) solutions were also used as controls (C-4 and C-5, respectively). The plates were incubated at 37 °C for 24 h and zone of inhibition (ZOI) were measured. The experiments were performed in triplicates. The mean of three replicates of the diameter of the ZOI was represented with standard deviation.

Minimal inhibitory concentration (MIC), representing the lowest concentration of antimicrobial agents that visually inhibits 99% growth of the microorganisms, was determined by the serial dilution method. The various concentrations (in triplicates) of AgNPs (100, 50, 25, 12.5 and 6.25 μg mL^{-1}) and of AuNPs (180, 90, 45, 22.5, 11.25 μg mL^{-1}) were tested for MIC measurement.

2.6.2. Brine shrimp (cytotoxicity) assay

This assay was performed by the study of the effect of different concentrations on survival and mortality of brine shrimp (*Artemia salina*) [25]. The brine shrimp eggs (1.0 g) in brine (320 g L^{-1}) were diluted with distilled water upto 1.0 L and incubated at 28 °C for 48 h in light. The AgNPs (10 and 30 nm 100, 50, 25, 12.5 and 6.25 μg mL^{-1}) and AuNPs (10 and 30 nm: 180, 90, 45, 22.5 and 11.25 μg mL^{-1}) containing the arabinoglucan were used. Each sample (2.0 mL) was diluted to 4.0 mL with brine. To this 10 numbers of the hatched shrimps were added. The control contained the brine (2.0 mL) diluted to 4.0 mL with water. The mixtures were incubated for 48 h in light and nauplii were counted by use of a magnifying glass. The results were reported as % mortality.

2.6.3. Cytotoxicity assay against HeLa cell line

This assay was performed according to a reported method [26,27]. Briefly, HeLa cells (1×10^4 cells, ATCC: CCL 2) were suspended with DMEM, FBS (10%), glucose (4500 mg L^{-1}) and of penicillin-streptomycin (1%) cover in 96-well plates. To this arabinoglucan, (670 μg mL^{-1}) and various concentrations of AgNPs (10 nm: 50, 25 and 12.5 μg mL^{-1}) and AuNPs (10 nm: 180, 90 and 45 μg mL^{-1}) were added in 1:1 ratio and cells were incubated again for further 24 h. Similarly the control cells were incubated without adding the NPs. After incubation the cells were isolated and washed with phosphate buffer saline (PBS) followed by addition of NR media and incubation for 2 h. The cells were isolated and washed with PBS and de-staining solution (glacial acetic acid-ethanol-water in 1:49: 50 ratio) was added. Optical density of the supernatant was recorded at 570 nm. The % viability was calculated according to the formula:

$$\text{Cell viability } (\%) = \frac{\text{sample absorbance}}{\text{control absorbance}} \times 100$$

The morphological changes in the cells were viewed and recorded by use of an inverted phase contrast microscope (CTR6000, Leica, Wetzlar, Germany).

2.6.4. Potato disc (anti-tumour) assay

This assay was performed according to the previously reported method Without any modification [17]. The solutions used were: arabinoglucan (670, 335, 167.5 μg mL^{-1}); AgNPs (25 and 10 nm: 50, 25 and 12.5 μg mL^{-1}) and AuNPs (30 nm and 10 nm: 180, 90 and 45 μg mL^{-1}). The results were reported as % inhibition according to the formula:

$$\%\text{Inhibition} = \frac{\text{Number of tumours in sample}}{\text{Number of tumours in control}} \times 100$$

2.6.5. Phytotoxicity assay

The phytotoxicity assay was performed by using radish seeds (*Raphanus sativus* L.) according to a reported method [28]. In this assay root length and the percent seed germination were determined. Briefly, the solutions (2.0 mL) of AgNPs (10 and 30 nm: 100, 50 and 25 μg mL^{-1}) and AuNPs (10 and 30 nm: 180, 90 and 45 μg mL^{-1}) were transferred to sterile Whatman 1 filter papers placed in sterile plates. The hemicellulose (670 and 335 μg mL^{-1}) and water were used as controls. Ten radish seeds were placed in each plate. The plates were incubated at 25 ± 2 °C in dark and root length was measured for 5 days and compared with the controls.

In another experiment two different concentrations of AgNPs (10 and 30 nm: 100, 50 and 25 μg mL^{-1}) and AuNPs (10 and 30 nm: 180, 90 and 45 μg mL^{-1}) along with two dilutions of hemicellulose as control (670 and 330 μg mL^{-1}) were used to determine the percent seed germination under similar conditions. The germination was recorded for 5 days. These experiments were performed in triplicate and data was statistically analysed.

2.7. Statistical analysis

The statistical analysis was performed by MS Excel® 2010 at $p < 0.05$ significance level.

3. Results and discussion

3.1. Total phenolic content

In order to rule out the redox activity, possibly, due to phenolic substances usually present in hemicelluloses the phenolic content of Ara-Glc was determined. It was found that the sample contained negligible amount (<100 ppm) of phenol. So, it was confirmed that the redox potential of the Ara-Glc was solely due to the functionalities in the hemicellulose itself.

3.2. Cyclic voltammetry of Ara-Glc

The cyclic voltammograms of the Ara-Glc under investigation and its major monomer component glucose are shown in Fig. 1. The peak potentials at 1.866 mV (anodic) and 1.802 mV (cathodic) were observed for the Ara-Glc, which match the values of glucose i.e. 1.780 mV (anodic) and 1.735 mV (cathodic). This clearly indicates that the functionalities in the Ara-Glc are oxidized and reduced reversibly. The shape of the voltammograms suggest a one-electron transfer process. This implies that the Ara-Glc is responsible for the reduction of the Ag^+ (+0.80 mV) and Au^{3+} (+1.50 mV) ions. This provides first direct evidence that any polysaccharide inherently possess reducing property. Based on this evidence a mechanism for the reduction process is suggested as shown in Scheme 1. This mechanism is supported by the fact that polysaccharides are hydrolysed by acids and alkalis (at high temperature) to varying degree [29]. The initial pH values of the $HAuCl_4$ and $AgNO_3$ solutions were 3.2 and 4.3, respectively, which were raised appropriately using the NaOH solution.

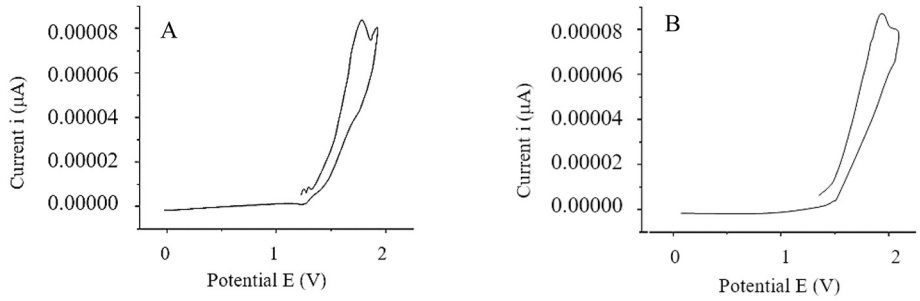

Fig. 1. Cyclic voltammograms: (A) glucose that is major monomer and (B) Ara-Glc @ 20. mVs^{-1}.

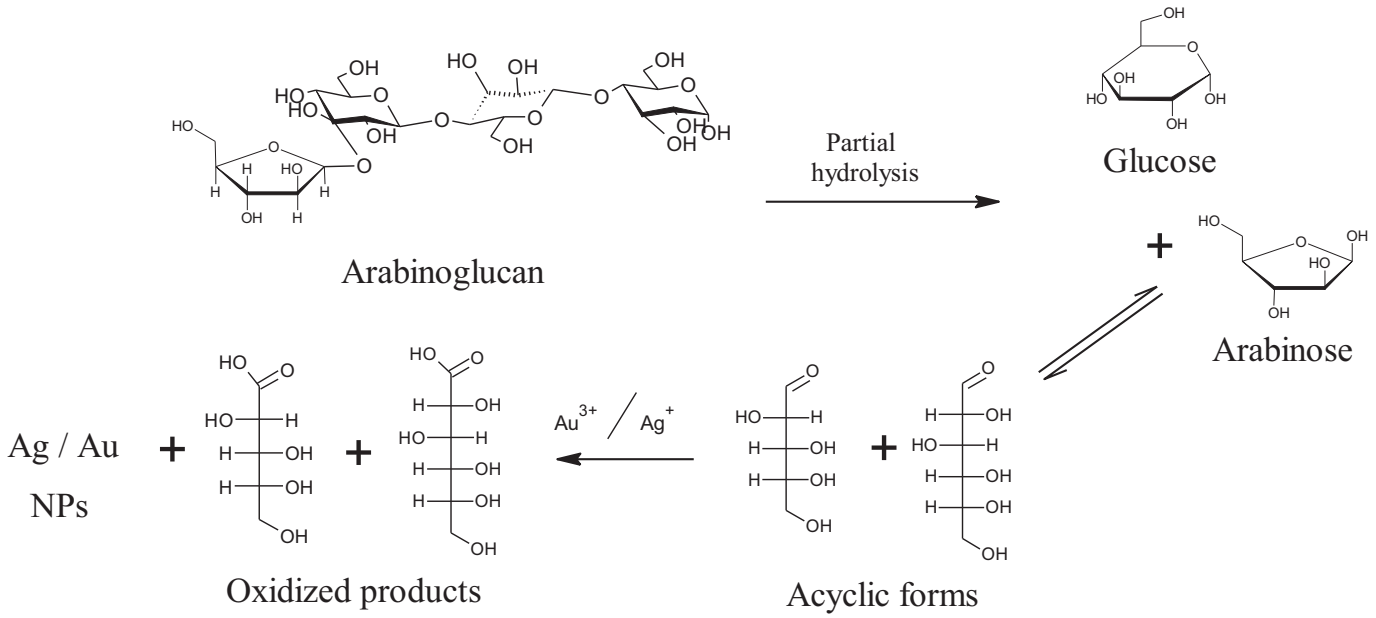

Scheme 1. Suggested mechanism for partial hydrolysis of hemicelluloses followed by reduction of metal ions.

3.3. Synthesis of NPs

The particles were readily formed by using Ara-Glc suspension 20 mL (0.2% w/v) at 90 °C and pH 8 for AuNPs and 20 mL at 90 °C and pH 10 for AgNPs. The formation of particles was witnessed by change in colour and confirmed by SPR absorptions at 512–528 nm (AuNPs) and 397–415 nm (AgNPs). The optimum reaction conditions were found to be: for AuNPs: Ara-Glc 0.2% w/v (20 mL/40 mL of 1.0 mM $HAuCl_4$), pH 8, temp. 90 °C; for AgNPs: Ara-Glc 0.2% w/v (20 mL/40 mL of 1.0 mM $AgNO_3$), pH 10, temperature 90 °C. The particle size and shape is highly dependent on these parameters [29]. In this case the reduction occurred without addition of chemical reducing and stabilizing agents and the particles thus produced dispersed in the polymeric matrix of Ara-Glc and stabilized. Hemicelluloses are polyhydroxylated compounds with at least one hemiacetal reducing end that can be oxidized easily in the presence of oxidizing metal ions. The isolated Ara-Glc has been characterized to contain aldoses; hexoses and pentoses [19] that are reducing sugars; therefore, they can reduce gold and silver ions with high positive reduction potential [30,31]. Moreover, hemicelluloses are also swellable and have capability to disperse NPs in their networks. Voids in the polymer network facilitate nucleation of the NPs and provide for a constrained environment [32]. The reduction reaction is thermodynamically possible if redox potential of the reducing agent is more negative than that of the metallic species. Thus, strongly electropositive metals like Au, Pt, Pd, Ag, Rh ($E° > 0.7$ V) can be reduced even with mild reducing agents under ordinary conditions.

3.4. Characterization of NPs

3.4.1. SPR spectra

The SPR spectra of AuNPs exhibited maxima from 512 to 528 nm (Fig. 2A and C) in different experiments depending upon the reaction parameters (the amount of Ara-Glc, pH and temperature). The lowest SPR maximum value achieved was 512 nm corresponding to a size of ~5 nm as calculated by Haiss equations (Eq. (2)). The SPR spectra of AgNPs started building up at pH > 6 and exhibited SPR maxima, which varied from 397 to 415 nm with reaction conditions (Fig. 2B and D). The lowest maximum at 397 nm represents the particle size <8 nm [23]. As the size of the NPs was affected by the amount of Ara-Glc, pH and temperature, the reaction conditions were optimized to obtain the smallest possible size of the particles. The synthesized particles were found to be stable for about four years (the time of last measurement) as no significant change in the position and intensity of the SPR maxima was observed. The exceptional high stability of the NPs is attributed to the effective encapsulation by the hemicellulosic material as observed earlier [9]. Hemicelluloses have branched structure with voids wherein the particles are trapped and stabilized.

3.4.2. X-ray diffraction

The pXRD spectra of the synthesized AuNPs and AgNPs produced at optimum conditions are shown in Fig. 3A and B. The spectra are characteristic of face-centered cubic phase (JCPDS File No. 87-0720). The diffraction peaks in the spectrum of AuNPs at 2θ values 32.81°, 40.72°

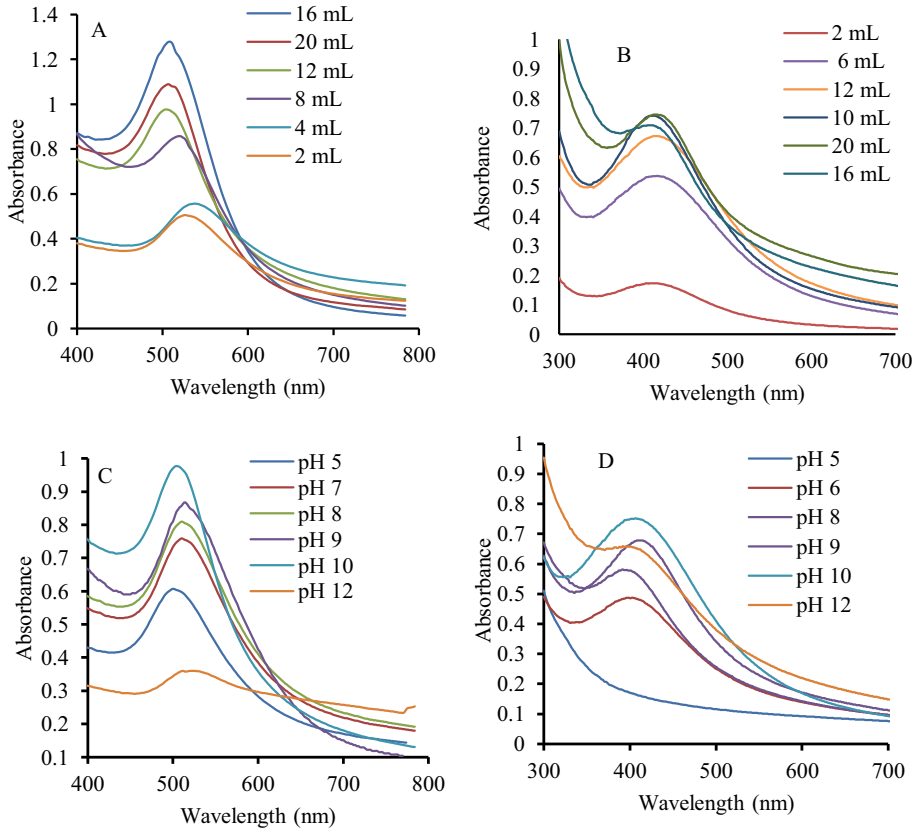

Fig. 2. SPR spectra: (A) AuNPs and (B) AgNPs with varying amount of Ara-Glc suspension (pH 8, 90 °C). SPR spectra: (C) AuNPs and (D) AgNPs at various pH (Ara-Glc: 20 mL, $HAuCl_4$: 20 mL, 90 °C).

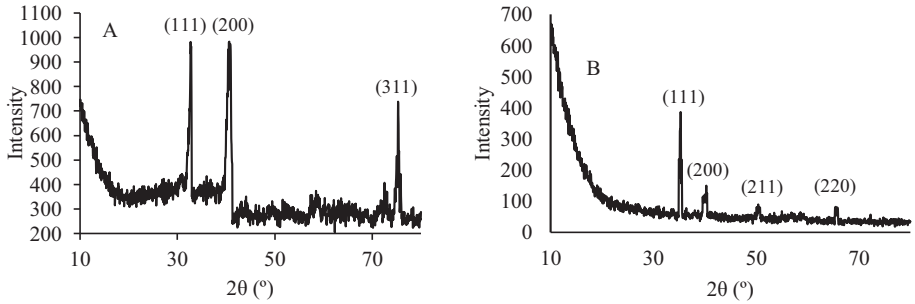

Fig. 3. XRD images: (A) AuNPs and (B) AgNPs.

and 75.5° can be assigned to (1 1 1), (200) and (3 1 1) planes respectively. Similarly in the AgNPs the 2θ values 35.3°, 40.45°, 50.72° and 65.9° can be assigned to (11 1), (2 0 0), (211) and (220) planes respectively. The sizes of the particles as calculated by Scherrer equation [33] were 4 nm and 8 nm for silver and gold, respectively.

3.4.3. Electron microscopy

SEM images (Fig. 4A and B) revealed that particles were almost uniform in size. EDX spectra (Fig. 4C and D) confirmed the presence of specific metal particles. Copper was additionally detected because of the use of copper grid in taking the images. The TEM images of NPs obtained under optimum conditions are shown in Fig. 4E and F. The particles exhibit almost spherical shapes. From these data the sizes of the particles were determined. The smallest particle sizes obtained under optimum conditions were ~6 nm and ~5 nm of Ag and Au respectively. These results are consistent with the SPR and XRD data (Table 2). It may be noted that the Ara-Glc under investigation produces smaller size particles than those produced by *arabinoxylan* and *glucoxylan* as reported previously [9,10]. This variation in the property of hemicelluloses may be anticipated due to their structural variations. The structure of Ara-Glc consists of hexoses as the major component and is highly branched as compared with arabinoxylan and glucoxylan [15]. This study highlights that the particle size can be controlled by use of an appropriate hemicellulose material.

AFM images were obtained as shown in Fig. 4C. It was observed that surface roughness of the Ara-Glc film increased after dispersion of NPs in the network. From the micrographs of the washed NPs (Fig. 4) it was possible to determine polydispersity of the particles. On the average the particles were found to be monodispersed with slight variation due to aggregation of the particles in some areas.

3.4.4. Zeta potential (ζ) measurements

Zeta potential (ζ) is a measure of an overall charge on the particles in a medium and it represents stability of the particles such that the higher

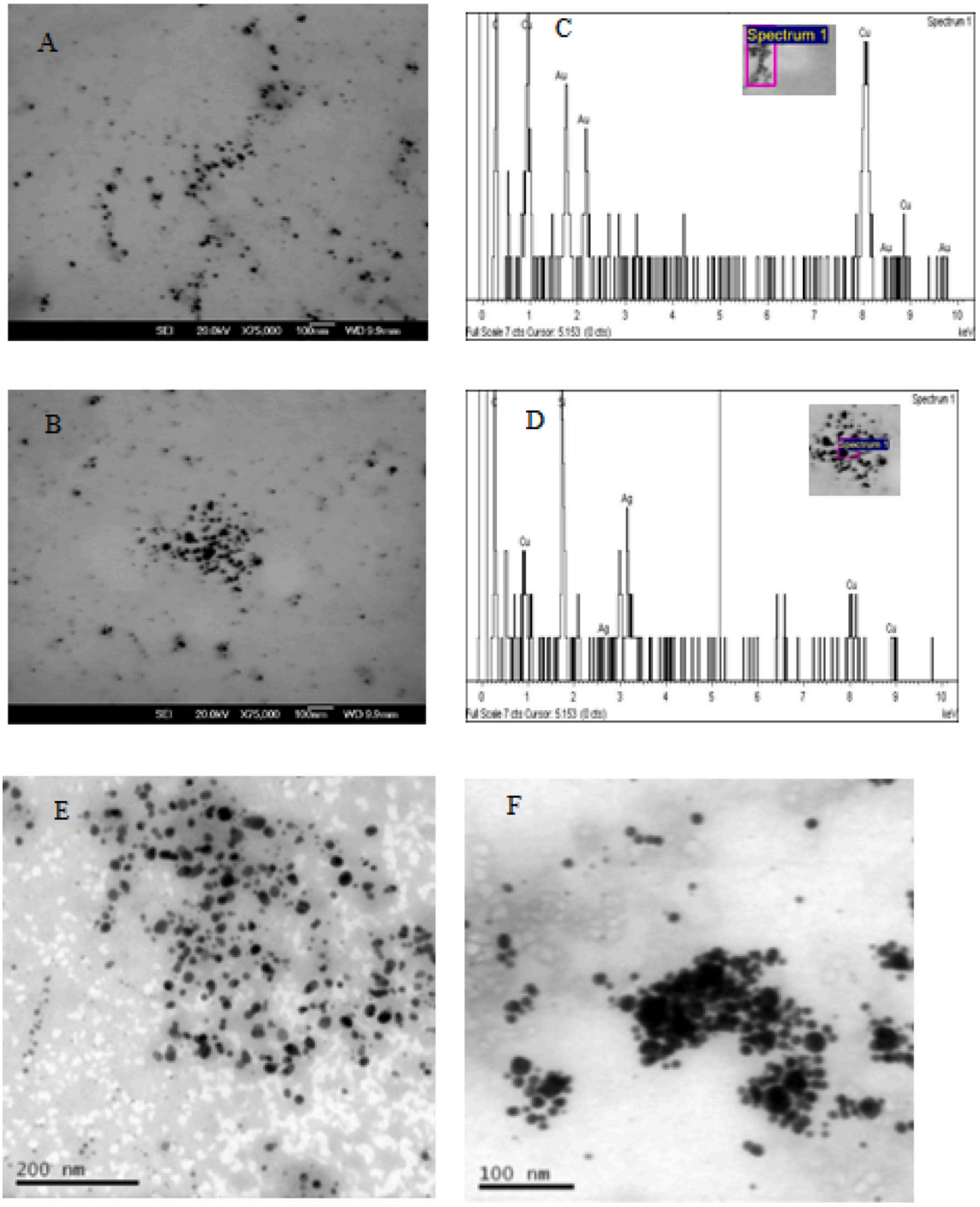

Fig. 4. SEM images: (A) AuNPs and (B) AgNPs dispersed in Ara-Glc suspension deposited on a carbon coated grid. EDX analysis: (C) AuNPs and (D) AgNPs. TEM images of particles dispersed in Ara-Glc suspension: (E) AuNPs and (F) AgNPs. (G) AFM images of AuNPs and (H) AgNPs deposited on silicon substrate.

the ζ value the more stable the particles will be [34]. The ζ values of synthesized NPs are listed in Table 1. NPs with ζ values greater than +25 mV or less than −25 mV typically have high degrees of stability. In this study the synthesized NPs exhibited higher ζ values in alkaline pH suggesting high stability. These values fall in the reported range for particles stable for a couple of years [35].

3.4.5. *Dynamic light scattering*

Hydrodynamic diameter and polydispersity index (PDI) of the NPs as determined by DLS measurements are listed in Table 1 and Fig. 5. At acidic pH the hydrodynamic diameter was of AuNPs was smaller than alkaline pH, whereas reverse behaviour was observed in case of AgNPs. The size measured by DLS technique represents the hydrodynamic diameter that is not only connected with the metallic core of the NPs (as is the case with microscopic techniques) but it is also influenced by the substances adsorbed on the surface of NPs. As a consequence, the size measured by DLS is always bigger than that by microscopic techniques [36]. In the present work the hydrodynamic diameters were 10–30 times bigger than those determined by electron microscopy probably due to the reason that the hemicelluloses have very high water holding

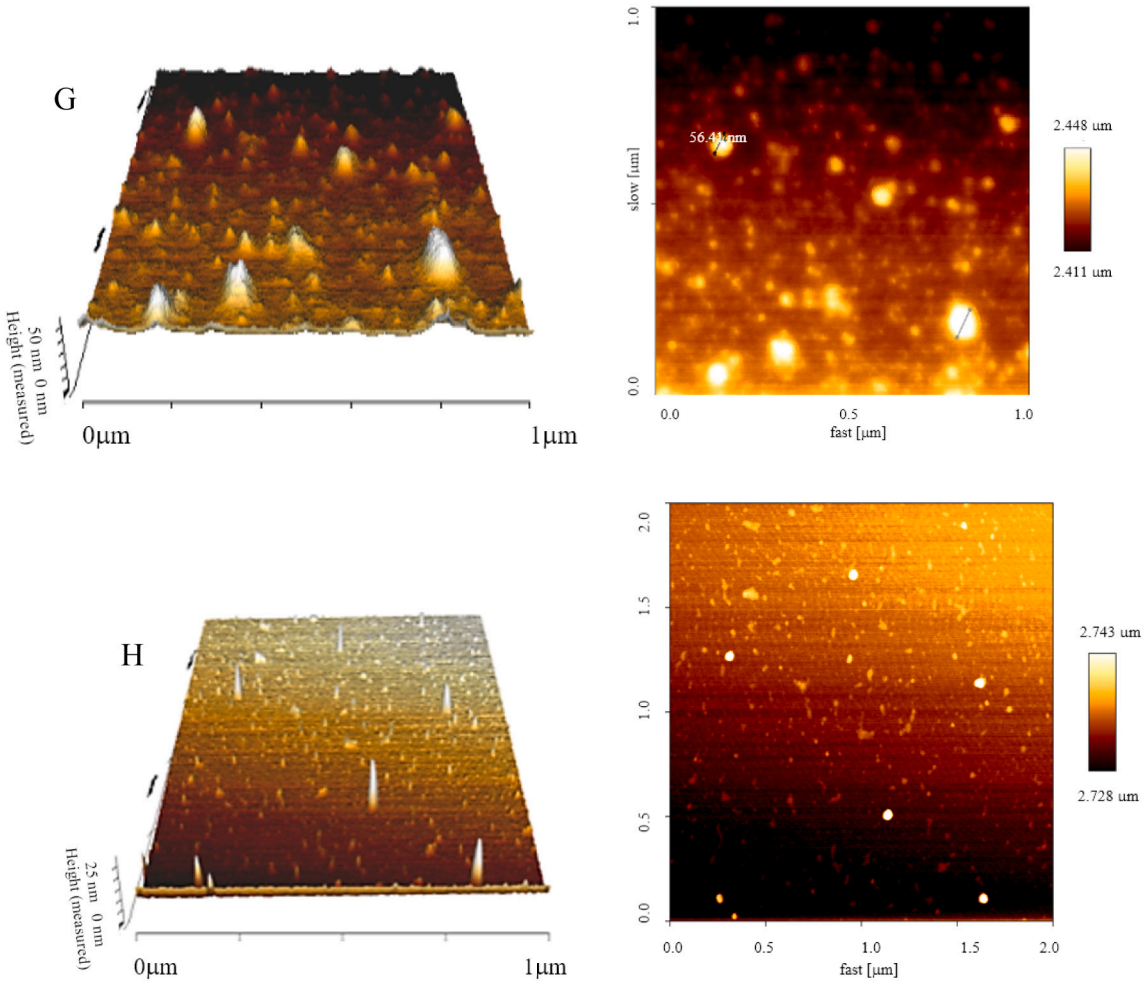

Fig. 4. (*continued*).

Table 1
Mean zeta potential, Z-average and PDI of the NPs (n = 10).

Sample	Zeta potential (ζ/mV)	pH	DLS Z-average (dia, nm)	PDI
AuNPs	−18.8 ± 1.9	6	93.27 ± 17.0	0.192
AuNPs	−24.3 ± 1.4	10	81.61 ± 40.2	0.352
AgNPs	−19.7 ± 5.81	7	111.7 ± 14.6	0.183
AgNPs	−22.1 ± 6.73	10	308.1 ± 22.0	0.128

Table 2
Size of NPs (produced at optimum conditions)[a] as determined by different techniques.

NPs	Size (nm): Ave ± SD (range)			
	SPR	XRD	TEM	DLS
AuNPs	15 ± 2 (5–60)	10 ± 2.3	10 ± 4.7 (5–35)	92.89 ± 8.22
AgNPs	8 ± 6 (5–40)	6 ± 3.7	10 ± 4.7 (5–20)	308.1 ± 22.06

[a] For AuNPs: Ara-Glc 0.2% w/v (20 mL/40 mL of 1.0 mM $HAuCl_4$), pH 8, temp. 90 °C; for AgNPs: Ara-Glc 0.2% w/v, (20 mL/40 mL of 1 mM $AgNO_3$), pH 10, temp. 90 °C.

capacity. As such the particles in the fully swollen matrix show up as big as observed here.

In DLS measurements PDI is a dimensionless number and scaled such that the maximum value is taken as 1.0, which indicates that the sample has a very broad size distribution and may contain large particles or aggregates that could be slowly sedimenting [37]. In the present work Ara-Glc from *LR* generally produced nearly monodisperse particles which may be attributed to uniform voids in the polymer matrix causing uniform nucleation for the NPs. The size distribution also depends on the nature of metal atoms; as it can be seen that in case of silver the PDI values are lower at alkaline pH as compared with those at acidic pH. In case of gold opposite behaviour was observed.

3.4.6. *Raman spectroscopy*

Raman spectra of the Ara-Glc with and without NPs (Fig. 6) showed the features of the glucan and indicated absence (no change in the band positions) of metal-glucan interaction. The prominent Raman frequencies and their assignments [38] were: 1718–1778 cm^{-1} (COO stretching) and 1566–1594 cm^{-1} (C═O), 1323–1392 cm^{-1} (HCC and HCO bending) and (CO stretching), 1247–1299 cm^{-1} (HCC and HCO bending), 1143–1196 cm^{-1} (heavy atom CC, CO stretching, HCC and HCO bending). It was noted that the broad bands at 1341 and 1553 cm^{-1} in the spectra of AgNPs dispersed in Ara-Glc, were enhanced in intensity significantly, which indicates that carboxylate group has been produced as a result of oxidation of the CH_2OH or the aldehyde group (in the acyclic structure of the sugar moieties) by silver ions [18]. In case of gold this effect was not visible. This finding is in line with several reports that AgNPs can be used as substrate for surface enhanced Raman scattering (SERS).

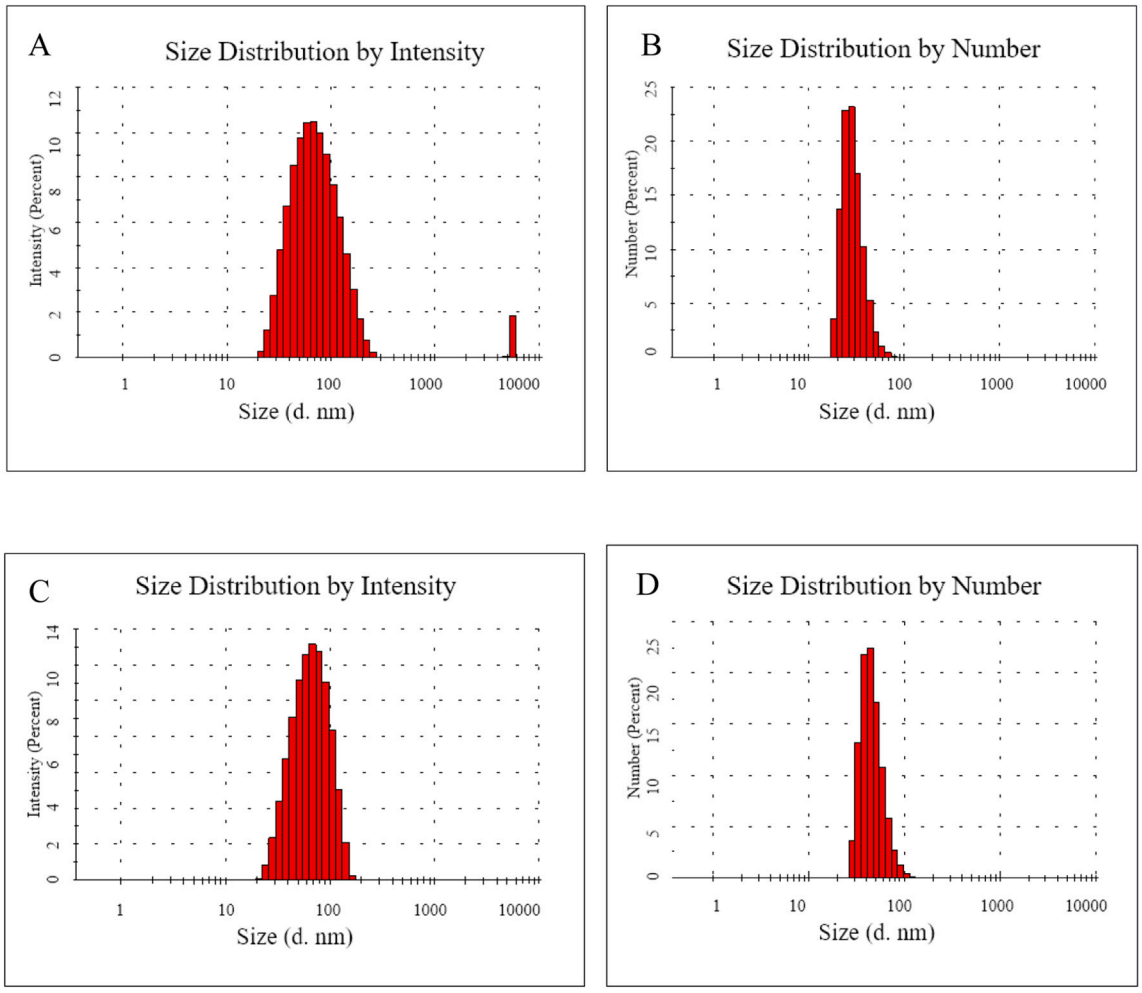

Fig. 5. Size distribution of particles dispersed in Ara-Glc measured by DLS technique (A) and (B) AuNPs. (C) and (D) AgNPs.

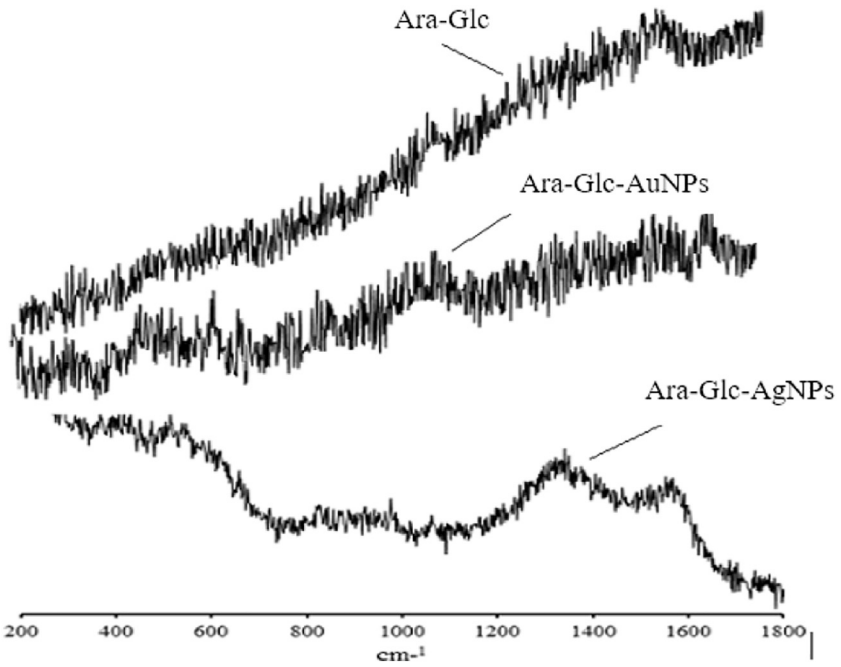

Fig. 6. Raman spectra of Au and AgNPs dispersed in Ara-Glc. Bands at 1341 and 1553 cm^{-1} in the spectra of AgNPs were enhanced in intensity significantly.

3.5. Bioassays

3.5.1. Antimicrobial assay

Antimicrobial activities of the synthesized NPs were graphed as shown in Fig. 7. The AgNPs displayed strong antimicrobial activity ($P < 0.05$) against *E. coli*, *A. tumefaciens*, *P. aeruginosa*, *B. subtilis* and *S. aureus*, whereas the AuNPs did not show any significant activity. This experiment suggests that the AuNPs having particle size between 10 and 30 nm are inactive and non-toxic [39] and as such are suitable for drug delivery. In case of AgNPs the antimicrobial activity varied in dose-dependent manner (Fig. 7B).The hemicellulose were used as control, which did not exhibit any significant activity. The activity of 10 nm particles was significantly greater than that of 30 nm particles as expected because of greater surface area per unit volume of the smaller particles [40,41]. *E. coli* were the most sensitive (MIC 6.25 μg mL^{-1}) to AgNPs followed by *P. aeroginosa* (MIC 10 μg mL^{-1}) and *S. aureus* (MIC 10 μg mL^{-1}). The MICs recorded in the present work were significantly lower than those reported by others [42,43] that can be explained due to high dispersion and thus greater surface area of the particles in the materials under investigation. Although, the exact mechanism regarding the antimicrobial activity of AgNPs is not known, several theories have been postulated thereof. AgNPs can anchor onto bacterial cell wall, react with it and perforate the membrane (pitting) leading to cell death [44]. An electron spin resonance study revealed that AgNPs produce free radicals when in contact with bacteria, that are responsible for cell death [45]. Another explanation could be that AgNPs penetrate into the cell wall and the nucleus and release the cell content [46,47]. Another possibility is rapid oxidation of particles to silver ions under physiological conditions [48,49].

3.5.2. Brine shrimp (cytotoxicity) assay

Brine shrimp assay provides a reliable test for cytotoxicity of metal NPs [50]. The AuNPs were found to be non-toxic as expected in this assay. The results of AgNPs are depicted in Fig. 8A and B. The highest mortality was shown by 10 nm AgNPs (12 ± 5.22 μg mL^{-1}). The mortality varied in a dose dependent manner ($P < 0.03$). Size of AgNPs was found to affect the cytotoxic activity; the smaller particles (10 nm) were more active as compared to larger particles (30 nm). This study also highlighted the role of hemicellulose used as stabilizing medium towards cytotoxic activity.

3.5.3. Cytotoxicity assay against HeLa cell line

Neutral red uptake assay provides a quantitative estimation of the number of viable cells in a culture. It is one of the widely used cytotoxicity tests for various drug molecules [26]. Results of this assay are shown in Fig. 9. In this assay 10 nm particles were used. The AuNPs did not show any significant activity, whereas AgNPs were active to different extent and the activity varied in a dose dependant manner (Fig. 9A). IC_{50} values of AgNPs (25 μg mL^{-1}). The cells treated with AgNPs at 100 and 50 μg mL^{-1} concentrations for 24 h showed significant morphological changes (Fig. 9C and D), which are characteristic features of apoptotic cells, such as loss of membrane integrity, cell shrinkage, and reduced cell density [51].

These results revealed that AgNPs could inhibit cell viability and induce membrane leakage in a dose-dependent manner. Various mechanisms for cytotoxic effects of silver have been described, which include physicochemical interaction of silver atoms with the functional groups of intracellular proteins, nitrogen bases an d phosphate groups in DNA [51]. Another suggested mechanism is that NPs can enter the cell through diffusion or endocytosis causing mitochondrial dysfunction,

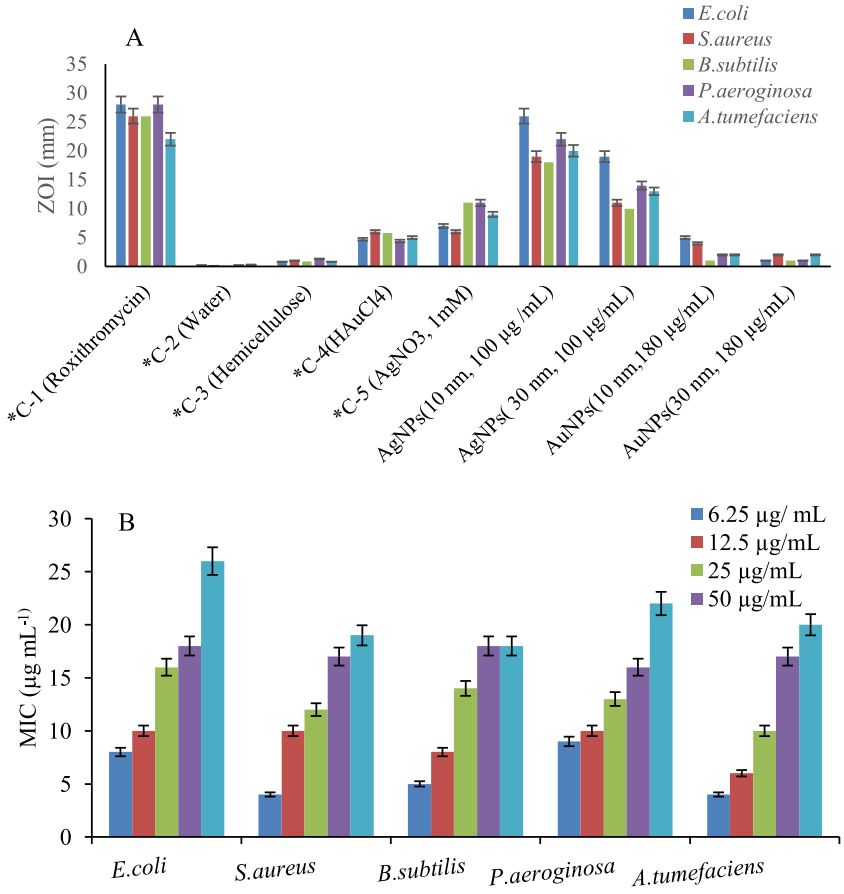

Fig. 7. (A) Antimicrobial assay of AuNPs and AgNPs. (B) MIC of AgNPs against different bacterial strains. Vertical bars indicate mean of three replicates ± standard deviation (SD).

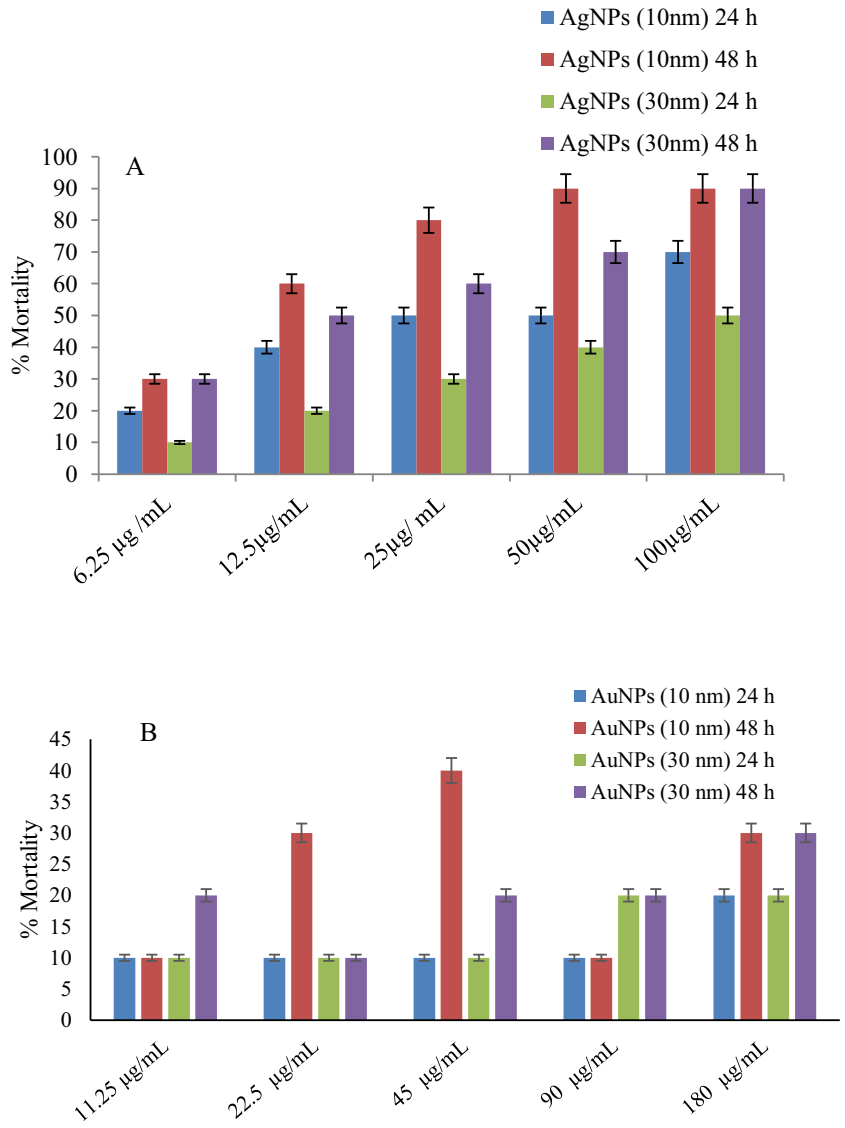

Fig. 8. (A) Cytotoxicity of AgNPs on *Artemia salina*: mortality of the larvae upto 100%. (B) cytotoxicity of AuNPs on *Artemia salina*: all the data were expressed in mean ± SD of three replicates ($P < 0.03$).

generation of reactive oxygen species (ROS), resulting in damage to proteins and nucleic acids inside the cells and finally inhibition of cell proliferation [52].

3.5.4. Potato disc (anti-tumour) assay

The potato disc bioassay is effective for screening antitumor activity. In this assay the tumour is induced by *Agrobacterium tumefaciens*, which is considered histologically similar to that in animals and humans [27,53,54]. The process of tumour induction by Ti-plasmid is the result of cell proliferation and blocking of apoptosis like in animal or human cancer cells. Results of this assay are shown in Fig. 10. AuNPs did not show any significant activity at all concentrations used. The activity of AgNPs varied in a dose dependant manner ($P < 0.05$). Smaller size of particles (10 nm) exhibited significantly higher activity as compared with that shown by larger particles (30 nm). IC_{50} values of AgNPs (30 µg mL^{-1}). The activity of AgNPs varied in a dose dependant manner ($P < 0.05$).

3.5.5. Phytotoxicity assay

The AgNPs and AuNPs exhibited different responses to seed germination and root length tests performed on the radish seeds. Both the AgNPs and AuNPs had no significant effect on seed germination. However, relatively higher germination as compared with control and comparable with that of the control (Ara-Glc) were observed (Fig. 11A), which may be attributed to the presence of highly hydrophilic component in polysaccharides. No significant effect of hemicellulose was observed in this test.

In the root length test AgNPs exhibited inhibitory effect at higher concentration (100 µg mL^{-1}) and enhanced the growth 5–6 times ($P < 0.05$) of the control (Fig. 11B) at a lower concentration (25 µg mL^{-1}). This phenomenon can be understood in terms of a possible sterilizing effect of the particles, which stimulates the growth, at lower concentration and toxic effect at higher concentrations. The stimulation effect may be on the cell division or cell length individually or collectively. As the enhanced root lengths were comparable in case of the particles having different sizes, it can be concluded that the effect of particle size is not significant. Previously a concentration dependent growth inhibition has been reported in other plants by AgNPs [55,56]. On the other hand, the AuNPs showed no significant effect in this test (Fig. 11) indicating that these particles are non-toxic to the plant under investigation. Therefore, the AuNPs produced by the present method, having an average size of ~30 nm and being non-toxic, can be safely used for

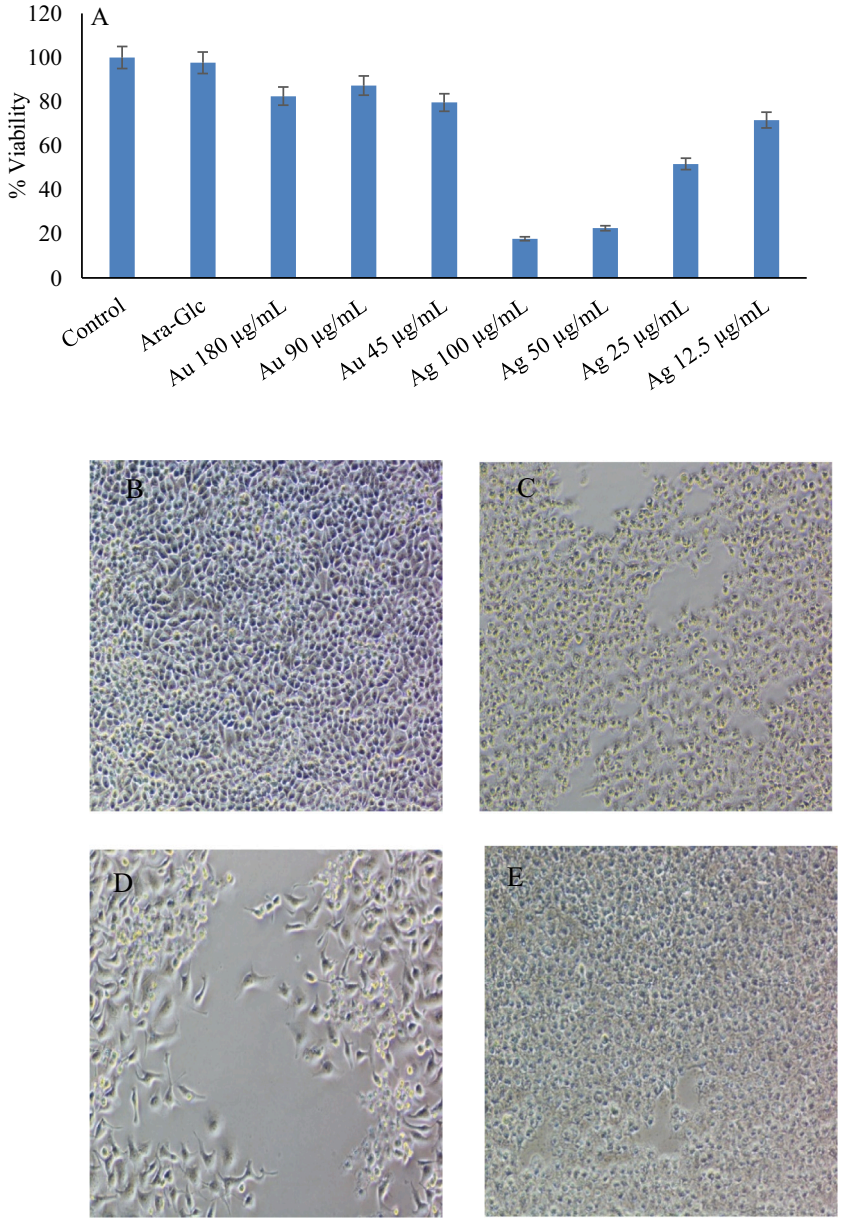

Fig. 9. (A) Cytotoxic effect of AuNPs (10 nm) and AgNPs (10 nm) against HeLa cell lines by neutral red assay; all the data were expressed in mean ± SD of three replicates ($P < 0.03$). Morphology of HeLa cell lines treated with: (B) hemicellulose (Ara-Glc), (C) AuNPs (180 µg mL^{-1}), (D) AgNPs (100 µg mL^{-1}) and e AgNPs (25 µg mL^{-1}) dispersed in hemicellulose. (For interpretation of the references to colour in this figure legend, the reader is referred to the web version of this article.)

drug delivery into the cells. Generally AuNPs proved to be non-toxic in all the bioassays performed in the present work. Therefore, these can be safely used for drug delivery and for diagnostic purposes. AgNPs were found to be potent and they exhibited a size- and dose-dependent activity against different pathogens, brine shrimp, HeLa cell line and plant tumour. AgNPs did not exhibit a significant activity in phytotoxicity test.

The antibacterial activity of 10 nm-AgNPs was comparable to that of roxithromycin and significantly higher than that of silver ions. No significant effect of hemicellulose, used in this work was observed in all the bioassays.

It can be concluded that AgNPs having size around 10 nm can be used for therapeutic effects against pathogens and tumours. It may be hypothesized that, due to their small size and larger surface area, 10 nm-AgNPs induce generation of ROS, which causes cell death. So they can be included in pharmaceutical formulations including wound dressings, antibacterial creams and ointments, bandages. They may also be employed as self-disinfecting coatings on medical devices and anti-fouling agents in garments. Another important use could be in water purification.

4. Conclusions

Highly stable gold and silver NPs were synthesized by use of arabinoglucan, a hemicellulose from *Lallemantia royleana* seeds, without use of additional reducing and stabilizing agents. This study demonstrates that the hemicellulosic material possesses inherent redox potential as verified by cyclic voltammetry. The particles were of small size (6–8 nm) and stable for about 4 years. The AuNPs were non-toxic, whereas the AgNPs exhibited pronounced antimicrobial and cytotoxic activities. The AgNPs showed potential to be used as probes in surface enhanced Raman spectroscopy as demonstrated by enhancement of Raman absorptions around 1341 and 1553 cm^{-1} in Raman spectra. The NPs embedded in arabinoglucan are suitable for biomedical applications as they absolutely free from hazardous residual reagents. The

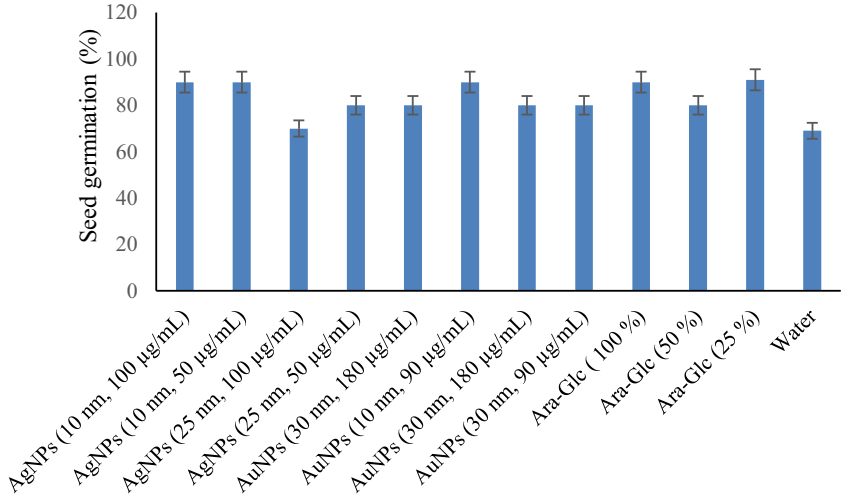

Fig. 10. Cytotoxic effect of AgNPs and AuNPs by % inhibition of crown gall tumour growth with varying concentration and size. AuNPs cytotoxicity was negligible with less than 20% inhibition. The data were expressed in mean ± SD of three replicates ($P < 0.05$).

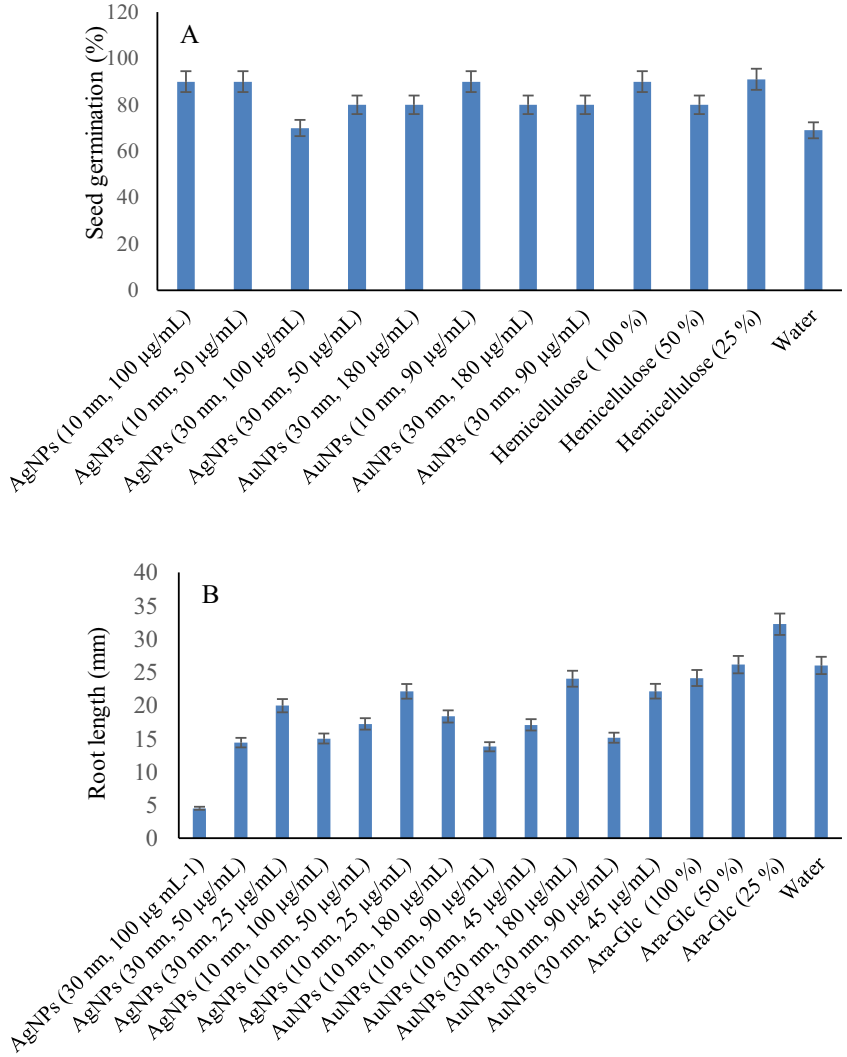

Fig. 11. Phytotoxicity assay: (A) effect of AgNPs and AuNPs with varying concentration and size on radish (%) seed germination. (B) Effect of AgNPs and AuNPs with varying concentration and size on the root growth of radish seeds. The data were expressed in mean ± SD of three replicates ($P < 0.05$).

hemicellulosic material used in this work is biodegradable, biocompatible and abundantly available at a very low cost.

CRediT authorship contribution statement

Fozia Iram: Methodology, Data curation, Original draft preparation. **Abida Yasmeen:** Methodology. **Shazma Massey:** Methodology. **Mohammad S Iqbal:** Conceptualization, Writing, Reviewing and Editing, Validation. **Sumreen Asim:** Methodology. **Misbah Irshad:** Methodology. **Hina Zahid:** Methodology, Data curation. **Athar Y Khan:** Data curation, Reviewing.

Declaration of competing interest

The authors declare that they have no competing interests.

References

[1] A. Shakeri-Zadeh, M. Ghasemifard, G. Ali Mansoori, Structural and optical characterization of folate-conjugated gold-nanoparticles, Phys. E 42 (2010) 1272–1280, https://doi.org/10.1016/j.physe.2009.10.039.

[2] K.L. Kelly, E. Coronado, L.L. Zhao, G.C. Schatz, The optical properties of metal nanoparticles: the influence of size, shape, and dielectric environment, J. Phys. Chem. B 107 (2003) 668–677, https://doi.org/10.1021/jp026731y.

[3] P. Khandelwal, A. Alam, A. Choksi, S. Chattopadhyay, P. Poddar, Retention of anticancer activity of curcumin after conjugation with fluorescent gold quantum clusters: an in vitro and in vivo xenograft study, ACS Omega 3 (2018) 4776–4785, https://doi.org/10.1021/acsomega.8b00113.

[4] B. Klębowski, J. Depciuch, M. Parlińska-Wojtan, J. Baran, Applications of Noble metal-based nanoparticles in medicine, Int. J. Mol. Sci. 19 (2018) 4031, https://doi.org/10.3390/ijms19124031.

[5] I. Karmous, A. Pandey, K. Ben Haj, A. Chaoui, Efficiency of the green synthesized nanoparticles as new tools in cancer therapy: insights on plant-based bioengineered nanoparticles, biophysical properties, and anticancer roles, Biol. Trace Elem. Res. 196 (2020) 330–342, https://doi.org/10.1007/s12011-019-01895-0.

[6] Y. Chen, X. Wang, Novel phase-transfer preparation of monodisperse silver and gold nanoparticles at room temperature, Mater. Lett. 62 (2008) 2215–2218, https://doi.org/10.1016/j.matlet.2007.11.050.

[7] G.H. Jeong, Y.W. Lee, M. Kim, S.W. Han, High-yield synthesis of multi-branched gold nanoparticles and their surface-enhanced raman scattering properties, J. Colloid Interface Sci. 329 (2009) 97–102, https://doi.org/10.1016/J.JCIS.2008.10.004.

[8] C. Deraedt, L. Salmon, S. Gatard, R. Ciganda, R. Hernandez, J. Ruiz, D. Astruc, Sodium borohydride stabilizes very active gold nanoparticle catalysts, Chem. Commun. 50 (2014) 14194–14196, https://doi.org/10.1039/c4cc05946h.

[9] M. Amin, F. Iram, M.S. Iqbal, M.Z. Saeed, M. Raza, S. Alam, Arabinoxylan-mediated synthesis of gold and silver nanoparticles having exceptional high stability, Carbohydr. Polym. 92 (2013) 1896–1900, https://doi.org/10.1016/j.carbpol.2012.11.056.

[10] F. Iram, M.S. Iqbal, M.M. Athar, M.Z. Saeed, A. Yasmeen, R. Ahmad, Glucoxylan-mediated green synthesis of gold and silver nanoparticles and their phyto-toxicity study, Carbohydr. Polym. 104 (2014) 29–33, https://doi.org/10.1016/j.carbpol.2014.01.002.

[11] F. Iram, M.S. Iqbal, I.U. Khan, R. Rasheed, A. Khalid, M. Khalid, S. Aftab, A. R. Shakoori, Synthesis and biodistribution study of biocompatible 198Au nanoparticles by use of arabinoxylan as reducing and stabilizing agent, Biol. Trace Elem. Res. (2019) 1–12, https://doi.org/10.1007/s12011-019-01700-y.

[12] H.B. Ahmed, M.A. Attia, F.M.S.E. El-Dars, H.E. Emam, Hydroxyethyl cellulose for spontaneous synthesis of antipathogenic nanostructures: (Ag & Au) nanoparticles versus Ag-Au nano-alloy, Int. J. Biol. Macromol. 128 (2019) 214–229, https://doi.org/10.1016/j.ijbiomac.2019.01.093.

[13] M.N. Belgacem, A. Gandini, Monomers, Polymers and Composites from Renewable Resources, 2008, https://doi.org/10.1016/B978-0-08-045316-3.X0001-4.

[14] A. Lazaridou, C.G. Biliaderis, M. Micha-Screttas, B.R. Steele, A comparative study on structure-function relations of mixed-linkage (1→3), (1→4) linear β-D-glucans, Food Hydrocoll. 18 (2004) 837–855, https://doi.org/10.1016/j.foodhyd.2004.01.002.

[15] F. Iram, S. Massey, M.S. Iqbal, D.G. Ward, Structural investigation of hemicelluloses from Plantago ovata, Mimosa pudica and Lallemantia royleana by MALDI-ToF mass spectrometry, J. Carbohydr. Chem. 37 (2018) 1–17, https://doi.org/10.1080/07328303.2018.1487973.

[16] G.N. Maity, P. Maity, I. Choudhuri, G.C. Sahoo, N. Maity, K. Ghosh, N. Bhattacharyya, S. Dalai, S. Mondal, Green synthesis, characterization, antimicrobial and cytotoxic effect of silver nanoparticles using arabinoxylan isolated from Kalmegh, Int. J. Biol. Macromol. 162 (2020) 1025–1034, https://doi.org/10.1016/j.ijbiomac.2020.06.215.

[17] F. Iram, M.S. Iqbal, I.U. Khan, R. Rasheed, A. Khalid, M. Khalid, S. Aftab, A. R. Shakoori, Correction to: synthesis and biodistribution study of biocompatible 198Au nanoparticles by use of Arabinoxylan as reducing and stabilizing agent, Biol. Trace Elem. Res. 193 (2020) 282–293, https://doi.org/10.1007/s12011-019-01723-5.

[18] M.S. Iqbal, S.J. Khurshid, M.Z. Iqbal, Preparation, characterization, and biologic evaluation of copper(II) – Schiff base complexes derived from anthranilic acid and aldoses, Can. J. Chem. 71 (1993) 629–633, https://doi.org/10.1139/v93-083.

[19] S. Massey, M.S. Iqbal, B. Wolf, I. Mariam, S. Rao, Comparative drug loading and release study on some carbohydrate polymers, Lat. Am. J. Pharm. 35 (2016) 146–155.

[20] J.D. Box, Investigation of the Folin-Ciocalteau phenol reagent for the determination of polyphenolic substances in natural waters, Water Res. (1983), https://doi.org/10.1016/0043-1354(83)90111-2.

[21] W. Haiss, N.T.K. Thanh, J. Aveyard, D.G. Fernig, Determination of size and concentration of gold nanoparticles from UV-vis spectra, Anal. Chem. 79 (2007) 4215–4221, https://doi.org/10.1021/ac0702084.

[22] P.K. Jain, K.S. Lee, I.H. El-Sayed, M.A. El-Sayed, Calculated absorption and scattering properties of gold nanoparticles of different size, shape, and composition: applications in biological imaging and biomedicine, J. Phys. Chem. B 110 (2006) 7238–7248, https://doi.org/10.1021/jp057170o.

[23] D. Paramelle, A. Sadovoy, S. Gorelik, P. Free, J. Hobley, D.G. Fernig, A rapid method to estimate the concentration of citrate capped silver nanoparticles from UV-visible light spectra, Analyst 139 (2014) 4855–4861, https://doi.org/10.1039/c4an00978a.

[24] S. Gummuluri, V.T. Kavalipurapu, A.V. Kaligotla, Antimicrobial efficacy of novel ethanolic extract of Morinda Citrifolia against Enterococcus feacalis by agar well diffusion method and minimal inhibitory concentration- an in vitro study, Braz. Dent. Sci. 22 (2019) 365–370, https://doi.org/10.14295/bds.2019.v22i3.1731.

[25] I. Varó, A. Perini, A. Torreblanca, Y. Garcia, E. Bergami, M.L. Vannuccini, I. Corsi, Time-dependent effects of polystyrene nanoparticles in brine shrimp Artemia franciscana at physiological, biochemical and molecular levels, Sci. Total Environ. 675 (2019) 570–580, https://doi.org/10.1016/j.scitotenv.2019.04.157.

[26] G. Repetto, A. del Peso, J.L. Zurita, Neutral red uptake assay for the estimation of cell viability/cytotoxicity, Nat. Protoc. 3 (2008) 1125–1131, https://doi.org/10.1038/nprot.2008.75.

[27] F. Iram, M.S. Iqbal, I.U. Khan, R. Rasheed, A. Khalid, M. Khalid, S. Aftab, A. R. Shakoori, Synthesis and biodistribution study of biocompatible 198 Au nanoparticles by use of Arabinoxylan as reducing and stabilizing agent, Biol. Trace Elem. Res. 193 (2019) 282–293, https://doi.org/10.1007/s12011-019-01700-y.

[28] M. Jamil, B. Mirza, A. Yasmeen, M.A. Khan, Pharmacological activities of selected plant species and their phytochemical analysis, J. Med. Plants Res. 6 (2012) 5013–5022, https://doi.org/10.5897/JMPR09.259.

[29] H. Huang, X. Yang, Synthesis of polysaccharide-stabilized gold and silver nanoparticles: a green method, Carbohydr. Res. 339 (2004) 2627–2631, https://doi.org/10.1016/j.carres.2004.08.005.

[30] M.M. Kemp, A. Kumar, S. Mousa, T.-J. Park, P. Ajayan, N. Kubotera, S.A. Mousa, R. J. Linhardt, Synthesis of gold and silver nanoparticles stabilized with glycosaminoglycans having distinctive biological activities, Biomacromolecules 10 (2009) 589–595, https://doi.org/10.1021/bm801266t.

[31] Y.N. Mata, E. Torres, M.L. Blázquez, A. Ballester, F. González, J.A. Muñoz, Gold(III) biosorption and bioreduction with the brown alga Fucus vesiculosus. - PubMed - NCBI, J. Hazard. Mater. 166 (2009) 612–618, https://doi.org/10.1016/j.jhazmat.2008.11.064.

[32] T. Trindade, Daniel-da-Silva Luísa, Advances in nanocomposite technology, Adv. Nanocomposite Technol. (2011) 275–291, https://doi.org/10.5772/676.

[33] A.L. Patterson, The scherrer formula for X-ray particle size determination, Phys. Rev. 56 (1939) 978–982, https://doi.org/10.1103/PhysRev.56.978.

[34] B.N. Ghosh, Evaluation of true zeta potential of the particles of an As2S3 sol in the presence of equicoagulating concentration of electrolytes, Trans. Faraday Soc. 49 (1953) 1477, https://doi.org/10.1039/tf9534901477.

[35] S. Rana, A. Bajaj, R. Mout, V.M. Rotello, Monolayer coated gold nanoparticles for delivery applications, Adv. Drug Deliv. Rev. 64 (2012) 200–216, https://doi.org/10.1016/j.addr.2011.08.006.

[36] E. Tomaszewska, K. Soliwoda, K. Kadziola, B. Tkacz-Szczesna, G. Celichowski, M. Cichomski, W. Szmaja, J. Grobelny, Detection limits of DLS and UV-Vis spectroscopy in characterization of polydisperse nanoparticles colloids, J. Nanomater. 2013 (2013) 60, https://doi.org/10.1155/2013/313081.

[37] C. Cascio, D. Gilliland, F. Rossi, L. Calzolai, C. Contado, Critical experimental evaluation of key methods to detect, size and quantify nanoparticulate silver, Anal. Chem. 86 (2014) 12143–12151, https://doi.org/10.1021/ac503307r.

[38] U.P. Agarwal, An overview of Raman spectroscopy as applied to Lignocellulosic Materials, in: Adv. Lignocellul. Charact, 1999, pp. 201–225. https://www.researchgate.net/publication/249994635.

[39] A.M. Alkilany, C.J. Murphy, Toxicity and cellular uptake of gold nanoparticles: what we have learned so far? J. Nanopart. Res. 12 (2010) 2313–2333, https://doi.org/10.1007/s11051-010-9911-8.

[40] J. Jiang, G. Oberdörster, A. Elder, R. Gelein, P. Mercer, P. Biswas, Does nanoparticle activity depend upon size and crystal phase? Nanotoxicology 2 (2008) 33–42, https://doi.org/10.1080/17435390701882478.

[41] Z. Ma, J. Liu, Y. Liu, X. Zheng, K. Tang, Green synthesis of silver nanoparticles using soluble soybean polysaccharide and their application in antibacterial coatings, Int. J. Biol. Macromol. 166 (2020) 567–577, https://doi.org/10.1016/j.ijbiomac.2020.10.214.

[42] Y. Zhou, Y. Kong, S. Kundu, J.D. Cirillo, H. Liang, Antibacterial activities of gold and silver nanoparticles against Escherichia coli and bacillus Calmette-Guerin, J. Nanobiotechnol. 10 (2012) 19, https://doi.org/10.1186/1477-3155-10-19.

[43] S.H. Kim, H.S. Lee, D.S. Ryu, S.J. Choi, D.S. Lee, Antibacterial activity of silver-nanoparticles against Staphylococcus aureus and Escherichia coli, Korean, J. Microbiol. Biotechnol. 39 (2011) 77–85.

[44] J.R. Morones, J.L. Elechiguerra, A. Camacho, K. Holt, J.B. Kouri, J.T. Ramírez, M. J. Yacaman, The bactericidal effect of silver nanoparticles, Nanotechnology 16 (2005) 2346–2353, https://doi.org/10.1088/0957-4484/16/10/059.
[45] S. Prabhu, E.K. Poulose, Silver nanoparticles: mechanism of antimicrobial action, synthesis, medical applications, and toxicity effects, Int. Nano Lett. 2 (2012) 1–10, https://doi.org/10.1186/2228-5326-2-32.
[46] J.S. Teodoro, A.M. Simões, F.V. Duarte, A.P. Rolo, R.C. Murdoch, S.M. Hussain, C. M. Palmeira, Assessment of the toxicity of silver nanoparticles in vitro: a mitochondrial perspective, Toxicol. in Vitro 25 (2011) 664–670, https://doi.org/10.1016/j.tiv.2011.01.004.
[47] A. Panacek, L. Kvítek, R. Prucek, M. Kolar, R. Vecerova, N. Pizúrova, V.K. Sharma, T. Nevecna, R. Zboril, Silver colloid nanoparticles: synthesis, characterization, and their antibacterial activity, J. Phys. Chem. B 110 (2006) 16248–16253, https://doi.org/10.1021/jp063826h.
[48] S. Hirn, M. Semmler-Behnke, C. Schleh, A. Wenk, J. Lipka, M. Schäffler, S. Takenaka, W. Möller, G. Schmid, U. Simon, W.G. Kreyling, Particle size-dependent and surface charge-dependent biodistribution of gold nanoparticles after intravenous administration, Eur. J. Pharm. Biopharm. 77 (2011) 407–416, https://doi.org/10.1016/j.ejpb.2010.12.029.
[49] W.-R. Li, X.-B. Xie, Q.-S. Shi, H.-Y. Zeng, Y.-S. Ou-Yang, Y.-B. Chen, Antibacterial activity and mechanism of silver nanoparticles on Escherichia coli, Appl. Microbiol. Biotechnol. 85 (2010) 1115–1122, https://doi.org/10.1007/s00253-009-2159-5.
[50] M.A. Maurer-Jones, S.A. Love, S. Meierhofer, B.J. Marquis, Z. Liu, C.L. Haynes, Toxicity of nanoparticles to brine shrimp: an introduction to nanotoxicity and interdisciplinary science, J. Chem. Educ. 90 (2013) 475–478, https://doi.org/10.1021/ed3005424.
[51] S. Gurunathan, J. Raman, S.N. Abd Malek, P.A. John, S. Vikineswary, Green synthesis of silver nanoparticles using Ganoderma neo-japonicum Imazeki: a potential cytotoxic agent against breast cancer cells, Int. J. Nanomedicine 8 (2013) 4399–4413, https://doi.org/10.2147/IJN.S51881.
[52] A. Haase, S. Rott, A. Mantion, P. Graf, J. Plendl, A.F. Thünemann, W.P. Meier, A. Taubert, A. Luch, G. Reiser, Effects of silver nanoparticles on primary mixed neural cell cultures: uptake, oxidative stress and acute calcium responses, Toxicol. Sci. 126 (2012) 457–468, https://doi.org/10.1093/toxsci/kfs003.
[53] F. Trigui, P. Pigeon, K. Jalleli, S. Top, S. Aifa, M. El Arbi, Selection of a suitable disc bioassay for the screening of anti-tumor molecules, Int. J. Biomed. Sci. 9 (2013) 230–236. http://www.pubmedcentral.nih.gov/articlerender.fcgi?artid=3884793&tool=pmcentrez&rendertype=abstract.
[54] C. Bodart, T. Lippeveld, R. Sauerborn, in: Chapter 1: Introduction, 1st, 2000, p. 14.
[55] E.J. Gubbins, L.C. Batty, J.R. Lead, Phytotoxicity of silver nanoparticles to Lemna minor L, Environ. Pollut. 159 (2011) 1551–1559, https://doi.org/10.1016/j.envpol.2011.03.002.
[56] W.-M. Lee, J. Il Kwak, Y.-J. An, Effect of silver nanoparticles in crop plants Phaseolus radiatus and Sorghum bicolor: media effect on phytotoxicity, Chemosphere 86 (2012) 491–499, https://doi.org/10.1016/j.chemosphere.2011.10.013.